SPECTROSCOPY-BASED METHOD FOR SENESCENT STUDY

Audi Putra Santosa

1st Year Master Student , ID: 685070045-4

Department of Microbiology, Faculty of Medicine, Khon Kaen University

Advisor: Assist.Prof. Wisitsak Phoksawat

Introduction: Senescence

➢ Senescence

Aging process on a cellular level.

Microscopic changes on our cells throughout our lifetime.

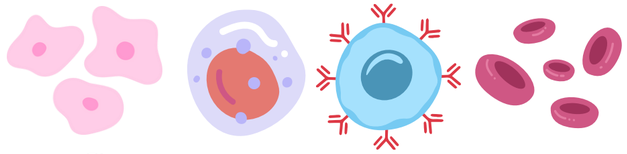

Senescence occurs on ALL CELLS!

➢ Immunosenescence (Immune+Senescence)

Age-related changes in the immune system

➢ Classification of aging (Immunology): 65 Years Old

Table 2.1
Number (in thousands) and proportion of persons aged 65 years and over by development group, 2023 and 2050

Region/year	*2023*		*2050*	
	Number	*Percentage*	*Number*	*Percentage*
Developed countries	258,311	20.2	351,500	27.8
ODCs	506,841	9.0	1,132,877	17.4
LDCs	42,637	3.7	118,566	6.1

LDC: Least Developed Countries; ODC: Other Developing Countries

Table 2.2
Number of countries with over 0.5 million persons aged 65 years and older, 2023 and 2050

Older persons aged 65 years and over	*2023*	*2050*
0.5-1 million	10	4
1-10 million	9	25
10 million and over	1	2
Total	**20**	**31**

Source: World Population Ageing 2023 (United Nations)

"WHO recognize ageing at the biological level can lead to gradual decrease in physical and mental capacity, increasing risk of disease and death."

Introduction: Immunosenescence

➢ Senescence on innate immune system:

- NK cells: Increase number CD56dim cells, reduced cytotoxicity, level of cytokines and chemokines reduced.
- Monocytes: Increase of absolute numbers, decrease in Toll-like Receptor (TLR) activation

➢ Senescence on adaptive immune system

- B cell: Decrease of antibody secretion capability
- T cell: defects in proliferation and effector functions

Effects of Immunosenescence?

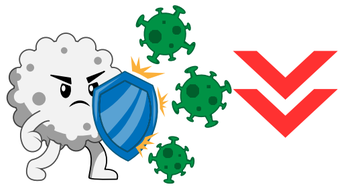

Immune response reduction

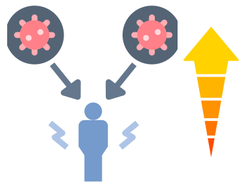

Increased infection susceptibility

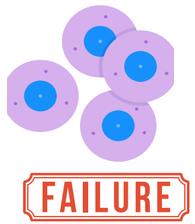

Cell proliferation failure

Accelerate disease development & progression

Lingering low grade inflammation

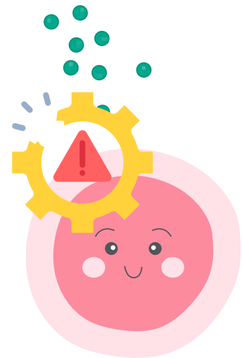

Spread of SASP protein to the normal structure and function of surrounding cells and tissues

*SASP: senescence-associated secretory phenotypes

Introduction: Pathogenic & Immunosenescent Cells

➢ What is this cells?

- Aberrent phenotype & functions
- Change in functions
- Progression into disease
- Immunosenescence

❖ CD4+CD28-NKG2D+ T cells (Pathogenic)

- High IL-17 producing, associated type 2 diabetes mellitus (T2DM) (Phoksawat et al., 2017)
- High IL-17 & IFN-γ producing, expanded in elderly (Phoksawat et al., 2020; Sornkayasit et al., 2021)

❖ CD4+CD57+ (high) CD28–T cells (Senescent)

- Associated with cardiovascular disease risk factors (Sornkayasit et al., 2025)

❖ CD39+CD8+ T cells (Pathogenic)

- ❖ Associated with Crohn's disease (Bai et al., 2015)
- ❖ PD-1 expressing, CD8+ T cells specific for HCV or HIV (Gupta et al., 2015)

Introduction: Biomarker & Technology to Senescence Detection

Biomarker?

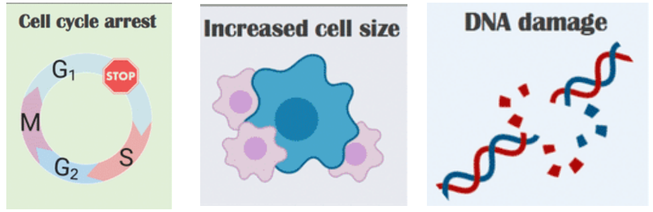

Source: https://pmc.ncbi.nlm.nih.gov/articles/PMC8038995/

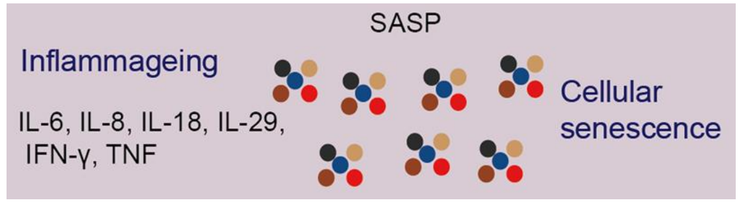

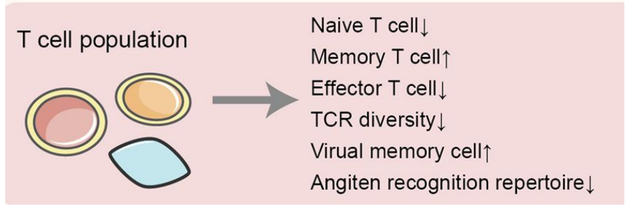

Source: https://www.nature.com/articles/s41392-023-01451-2#Sec2

BD Biosciences

Flow Cytometry:

- Directly measurement of expressing senescence markers

Limitations:

- Expertise
- Subjective analysis (gating)
- Cost & accessibility

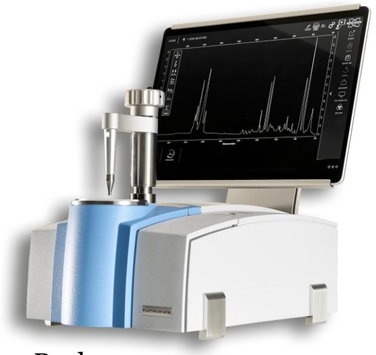

Bruker

FTIR:

- Label-free, non-destructive, to observe biochemical changes

Limitations:

- Water interference
- Poor spatial resolution

Raman Spectroscopy (Bruker, Edinburth Instruments)

Raman/SERS approach:

- Raman spectra follows sample composition
- Minimum sample preparation
- Specificity & Sensitivity: Fingerprint
- Versatile sample type

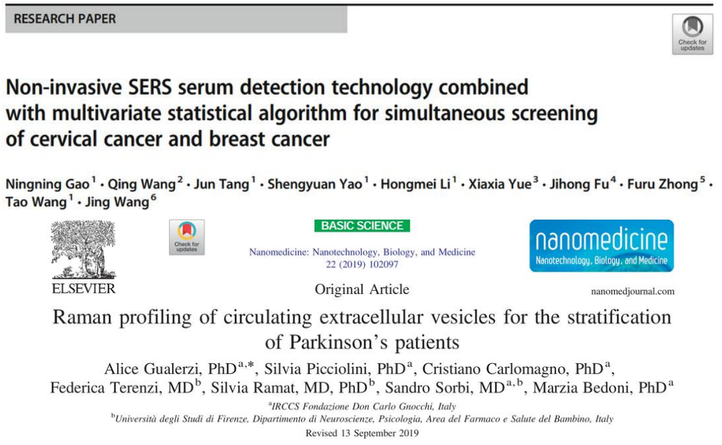

RESEARCH PAPER

Non-invasive SERS serum detection technology combined with multivariate statistical algorithm for simultaneous screening of cervical cancer and breast cancer

Ningning Gao[1] · Qing Wang[2] · Jun Tang[1] · Shengyuan Yao[1] · Hongmei Li[1] · Xiaxia Yue[3] · Jihong Fu[4] · Furu Zhong[5] · Tao Wang[1] · Jing Wang[6]

ELSEVIER

BASIC SCIENCE

Nanomedicine: Nanotechnology, Biology, and Medicine 22 (2019) 102097

Original Article

nanomedicine Nanotechnology, Biology, and Medicine

nanomedjournal.com

Raman profiling of circulating extracellular vesicles for the stratification of Parkinson's patients

Alice Gualerzi, PhD[a,*], Silvia Picciolini, PhD[a], Cristiano Carlomagno, PhD[a], Federica Terenzi, MD[b], Silvia Ramat, MD, PhD[b], Sandro Sorbi, MD[a,b], Marzia Bedoni, PhD[a]

[a]IRCCS Fondazione Don Carlo Gnocchi, Italy

[b]Università degli Studi di Firenze, Dipartimento di Neuroscienze, Psicologia, Area del Farmaco e Salute del Bambino, Italy

Revised 13 September 2019

Introduction: Raman/SERS Application

➢ Agriculture

Pesticides residues

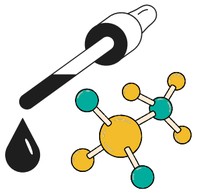

Chemical Additives: Dye

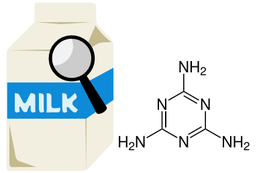

Melamine in dairy

➢ Pharmaceuticals

Identify components

Stability

Purity & Uniformity

➢ Art & Archaeology

Pigment & material identification

Degradation

Material analysis

➢ Medical Field

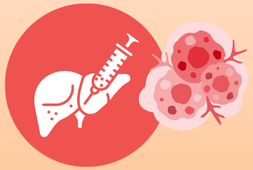

Biopsy: cancer

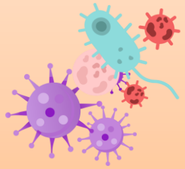

Pathogen

Neurological diseases

Immunosenescence?

Pathogenic cells?

Seminar Papers

Paper 1:

SJR 2024

1.670 Q1

H-INDEX

158

cells

MDPI

Article

Attenuated Total Reflectance-Fourier Transform Infrared (ATR-FTIR) Spectroscopy Discriminates the Elderly with a Low and High Percentage of Pathogenic CD4+ T Cells

Rian Ka Praja [1,2], Molin Wongwattanakul [2], Patcharaporn Tippayawat [2,3], Wisitsak Phoksawat [4,5], Amonrat Jumnainsong [2,6], Kanda Sornkayasit [2] and Chanvit Leelayuwat [2,6,*]

Paper 2:

SJR 2024

1.735 Q1

H-INDEX

86

Nanoscale Horizons

ROYAL SOCIETY OF CHEMISTRY

COMMUNICATION

View Article Online
View Journal | View Issue

Check for updates

Cite this: *Nanoscale Horiz.*, 2022, 7, 1488

Received 3rd May 2022,
Accepted 5th September 2022

DOI: 10.1039/d2nh00220e

rsc.li/nanoscale-horizons

Nanoscale biophysical properties of small extracellular vesicles from senescent cells using atomic force microscopy, surface potential microscopy, and Raman spectroscopy†

Hyo Gyeong Lee,‡[a] Seokbeom Roh,‡[bc] Hyun Jung Kim,[bd] Seokho Kim,[e] Yoochan Hong,*[d] Gyudo Lee*[bc] and Ok Hee Jeon*[a]

Paper 1: Overview Th Cells (CD4+)

Th Cells, CD4+:

- Activated by antigen recognition by MHC Class II molecule
- Coordinating immune response:
  - Cytokine secretion
- Develop long-lived memory cells

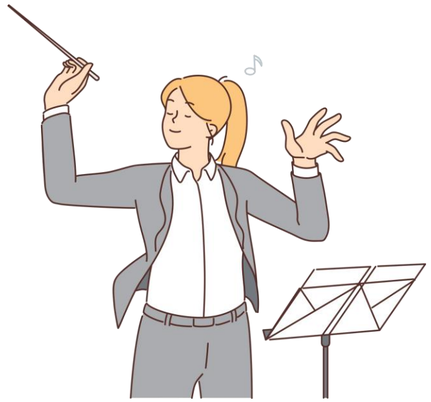

Th cells as “conductor”

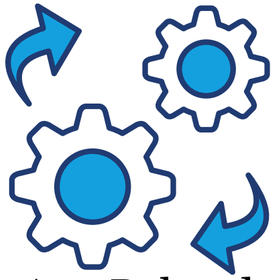

Age-Related

→

- Inappropriate T helper subset differentiation
- Diminished proliferative capacity
- Increase in regulatory T cells

→

T cell dysfunction:

Progression of disease

<u>Importance for Early Detection</u>

Paper 1: Overview

cells

MDPI

Article

Attenuated Total Reflectance-Fourier Transform Infrared (ATR-FTIR) Spectroscopy Discriminates the Elderly with a Low and High Percentage of Pathogenic CD4+ T Cells

Rian Ka Praja [1,2], Molin Wongwattanakul [2], Patcharaporn Tippayawat [2,3], Wisitsak Phoksawat [4,5], Amonrat Jumnainsong [2,6], Kanda Sornkayasit [2] and Chanvit Leelayuwat [2,6,*]

Objective:

- To discriminate the elderly groups with a low percentage and a high percentage of pathogenic CD4+ T cells by using machine learning-empowered ATR-FTIR.
- To investigate biochemical changes in serum, exosome, and HDL samples

High percentage (HP): ≥6%

Low percentage (LP): ≤3%

Sample size: 21LP & 22HP

Conditions observed in this study:

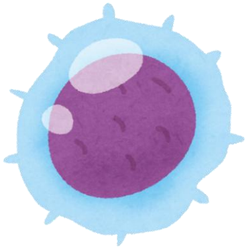

(Pathogenic CD4+ T-cells)

- CD28-
- NKG2D+
- High IL-17 producing cell

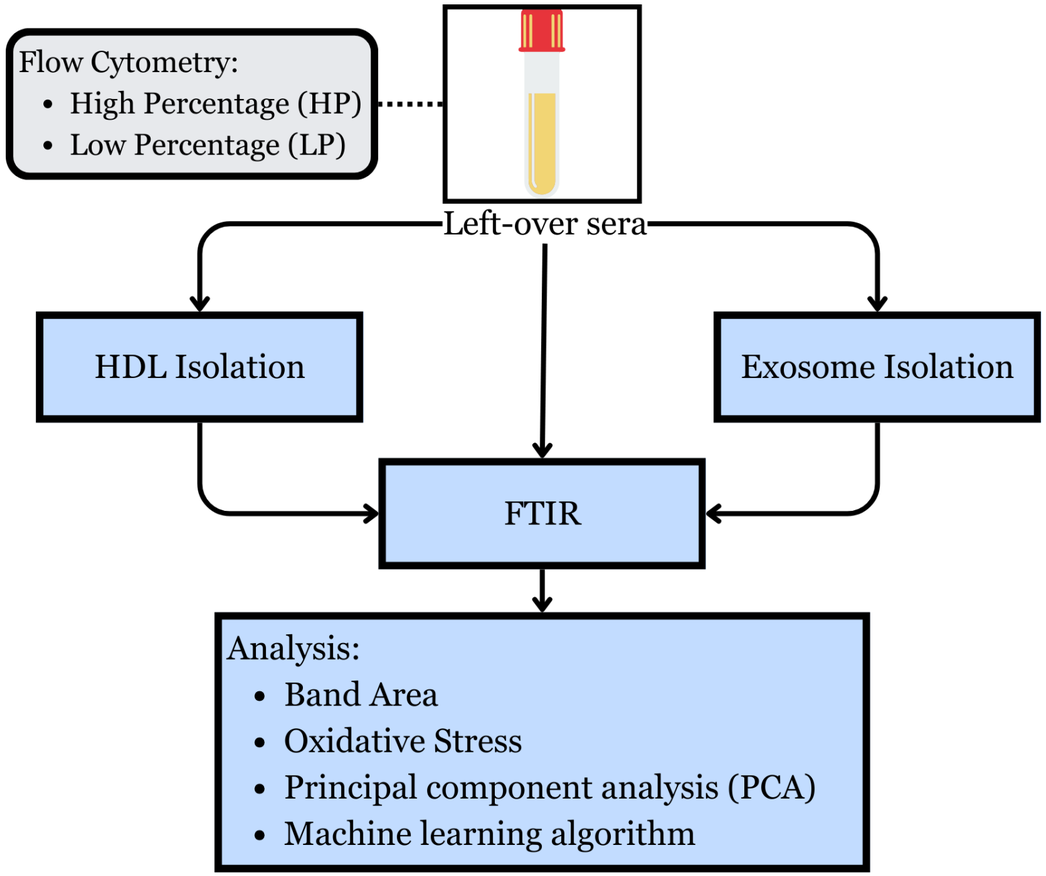

Paper 1: Materials and Methods

Sample preparation (1)

- High Percentage
- Low Percentage

CD4+CD28-NKG2D+ (pathogenic CD4+) T cells

Left-over sera

HDL Isolation
- HDL purification kit (Cell Biolabs)
- 200 µL serum

Exosome Isolation
- ExoQuick™ Exosome Precipitation Solution (System Biosciences)
- 50 µL serum

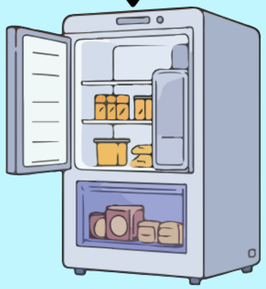

−80 ◦C storage

Spectral Acquisition & Analysis (2)

HDL — 3 µL

Serum — 3 µL

Exosome — 3 µL

Agilent 4500 FTIR spectroscopy

5 minutes

- Acquisition at 4000–650 cm^{-1}
- 64 scans
- Spectral resolution 4 cm^{-1}
- 3 measurements/sample

Raw Spectra

Baseline Correction & Normalization

Unscrambler

Unsupervised

Supervised

Machine Learning

SpectraGryph ... One App to treat them all ...

Biochemical Components

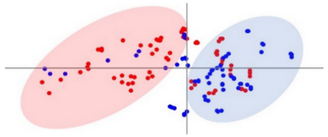

Separation Trend

% Accuracy, Sensitivity, Specificity, PPV, NPV

Result: Biomolecular Content Study by Spectral Band Area Analysis

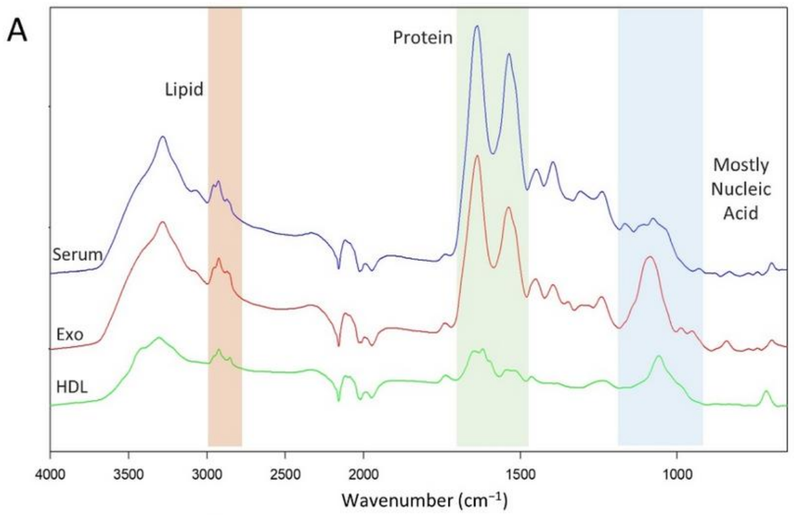

ATR spectra collected and compared:

- 3000–2800cm-1 (lipid)
- 1700–1500cm-1 (protein)
- 1270–960cm-1 (nucleic acid)

→ Exosome:
Lipid and nucleic acid contents inthe HP group were significantly higher than inthe LP group ($p<0.001$ and $p<0.01$)

→HDL:
Protein contents was significantly different between the HP and LP groups ($p<0.05$)

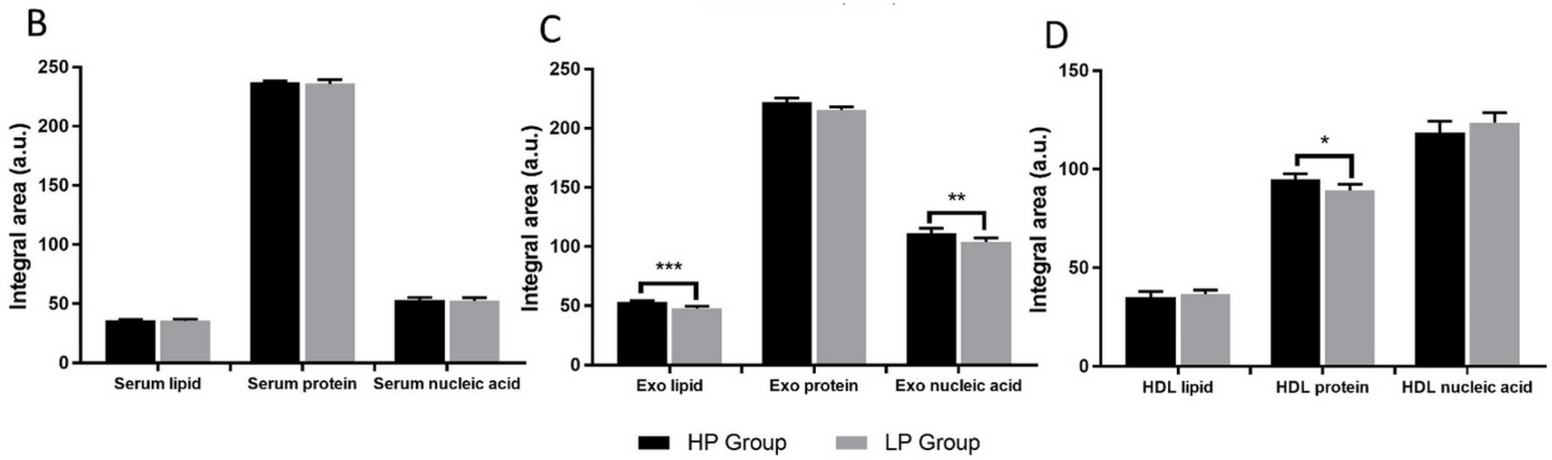

Figure 1. Results of spectral band area analysis of serum, exosome, and HDL spectra. Representative spectra from serum (blue), exosome (red), and HDL (green). Regions selected for the spectral band area analysis were 3000–2800 cm−1 lipid (orange region), 1700–1500 cm−1 protein (green region), and 1270–960 cm−1 nucleic acid (blue region) **(A)**. The comparison of spectral band area between the LP and HP groups based on serum **(B)**, exosome **(C)**, and HDL spectra **(D)**; * = $p < 0.05$; ** = $p < 0.01$; *** = $p < 0.001$.

There are difference in HP and LP group in exosome lipid, exosome nucleic acid, and HDL protein.

Suggests possible markers to differentiate between HP and LP.

*High percentage (HP): ≥6% , Low percentage (LP): ≤3%

Result: Differences between Spectra from the LP and HP Groups

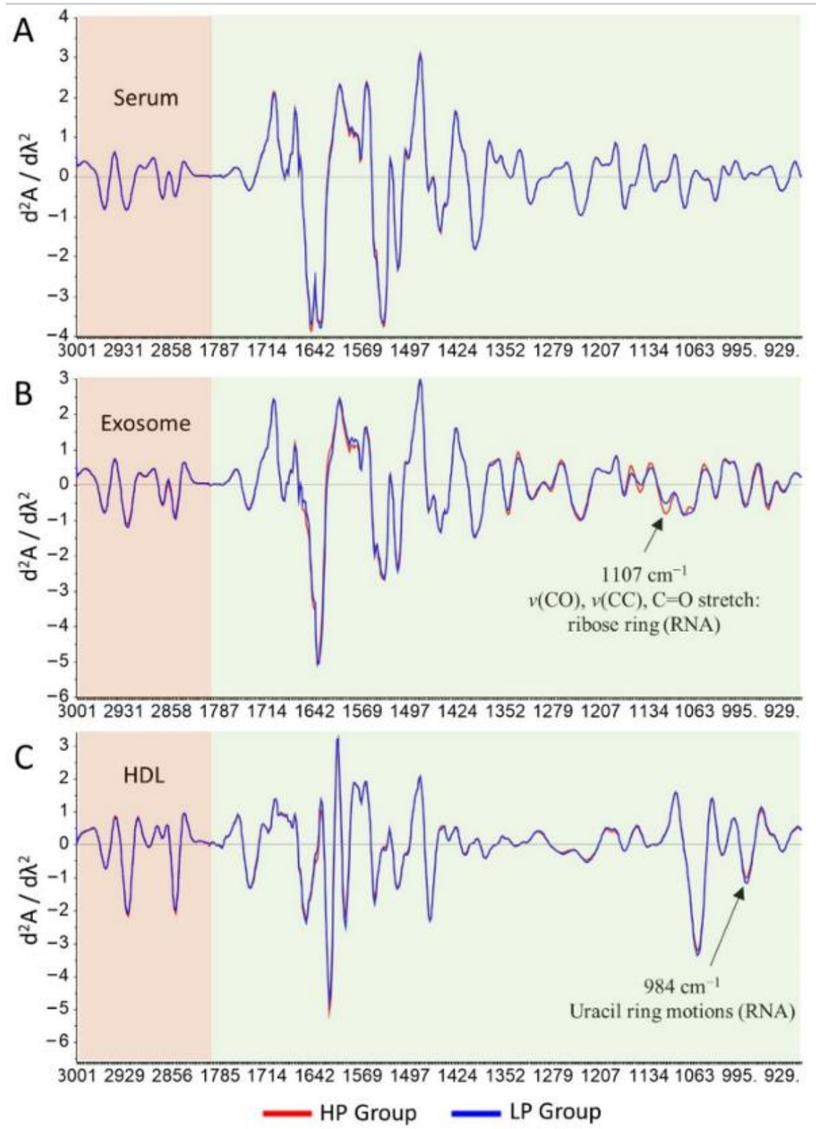

Absorbance bands:

Lipids (3000–2800 cm-1)	Protein/phospholipids/DNA/RNA/carbohydrate (1800–900 cm-1)

➢ Serum:

Similar between 2 groups

➢ Exosome:

- Only the band at 1107 cm^{-1} had significantly higher intensity in the HP compared to LP group
- Assigned to υ (CO) and υ (CC)

➢ HDL:

- Significant difference only at the band 984 cm^{-1}
- Assigned to uracil ring motions of RNA

Difference in the spectra between 2 group if exosome and HDL.

Might be possible to differentiate 2 group using these 2 sample types.

Figure 2. Averaged second derivative ATR-FTIR spectra with SNV normalization in the regions of 3000–2800 cm−1 (pale-pink box) and 1800–900 cm−1 (pale-grayish green box). Comparison of averaged second derivative spectra between LP and HP groups in serum (A), exosome (B), and HDL spectra (C). Comparison of band intensity was done by independent sample t-test. A significant difference in band intensity is depicted by the arrow (→). Blue and red represent the elderly groups with a low percentage (LP; ≤3%) and a high percentage (HP; ≥6%) of pathogenic CD4+ T cells, respectively.

*High percentage (HP): ≥6% , Low percentage (LP): ≤3%

Result: Discrimination by Unsupervised Analysis (Principal Component Analysis)

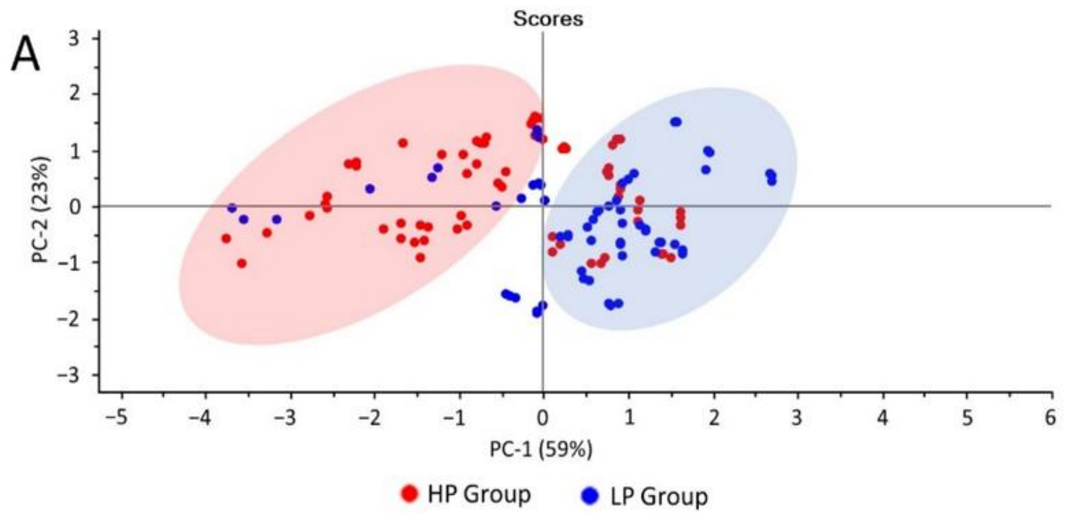

Figure 3. PCA analysis of the 1700–1500 cm^{-1} FTIR exosome spectral range. PCA score plots (**A**) and PCA loading plots (**B**). PCA score plots showed distinct clustering between the LP (blue box) and HP groups (pink box). PCA loading plots identify specific important peaks for the LP and HP groups.

Total of 129 serum, exosome, and HDL spectra analyzed:

- Lipid region (3000–2800 cm^{-1})
- Mixed region (1800–900 cm^{-1})
- Protein region (1700–1500 cm^{-1})
- Fingerprint region (1500–900 cm^{-1})

Wave-number around 1700–1500 cm^{-1} (protein) of exosome spectra showed a **possible separation** between the LP and HP groups.

The protein region could be used to discriminate between the LP and HP groups.

Unsupervised analysis give possible separation, but better analysis or algorithm might be better.

*High percentage (HP): ≥6% , Low percentage (LP): ≤3%

Result: Establishment of Partial Least Square Discriminant Analysis (PLS-DA) Model for Discrimination

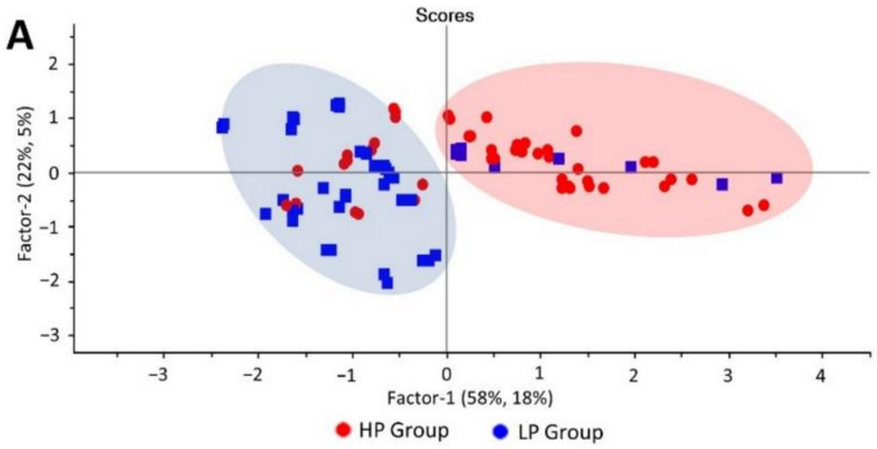

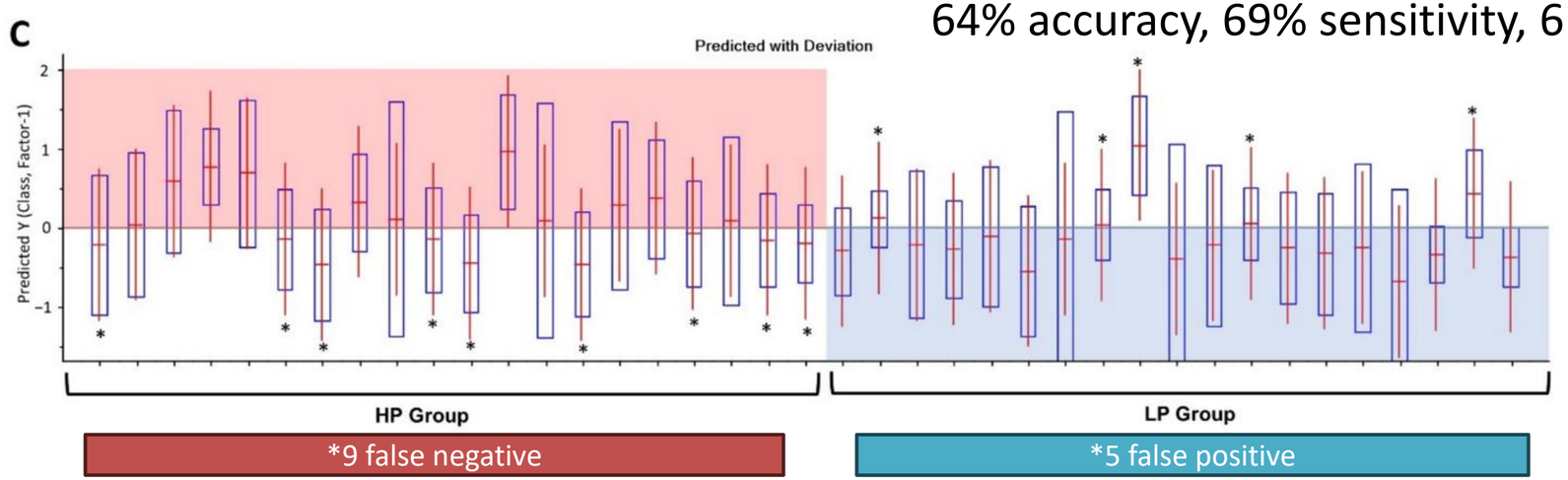

Figure 4. PLS-DA analysis results. A score plot of PLS-DA of the 1700–1500 cm−1 FTIR exosome spectral range (A), and predictive results of PLS-DA generated using the 1700–1500 cm−1 region (C). False predictions are depicted with stars (*). Nine false-negative and five false-positive predictions were identified with the PLS-DA predictive model.

*High percentage (HP): ≥6% , Low percentage (LP): ≤3%

Exosome spectra (1700–1500 cm^{-1}) divided into two datasets: training set and testing ; 70:30

- 90 spectra > training
- 39 spectra > testing

➢ PLS model generated gave a discrimination along with Factor-1 (x-axis).

Based on PLS model:

- HP group set to a positive value (+1)
- LP group was assigned to a negative value (−1)

➢ 14 false predictions

64% accuracy, 69% sensitivity, 61% specificity, 55% PPV, and 74%NPV

Discrimination using PLS-DA model could be observed but the performance of the PLS-DA model was not favorable enough.

Better classification model is needed.

Result: Classification Model Using Advanced Machine Learning Algorithms

Result: **Serum**; 70:30 for training and testing

Sample	Region (cm^{-1})	Algorithm	Performance				
			Acc (%)	Sens (%)	Spec (%)	PPV (%)	NPV (%)
Serum	3000–2800 Lipid	J48 Decision Tree	54	54	53	65	42
		RF	51	53	50	50	53
		SVM	44	46	38	60	26
		NN (4)	51	53	50	50	53
	1800–900 Mixed	J48 Decision Tree	72	80	67	60	84
		RF	92	100	86	85	100
		SVM	77	79	75	75	79
		NN (20)	100	100	100	100	100
	1700–1500 Protein	J48 Decision Tree	69	75	65	60	79
		RF	90	90	89	90	89
		SVM	62	58	75	90	32
		NN (14)	90	86	94	95	84
	1500–900 Fingerprint	J48 Decision Tree	56	60	54	45	68
		RF	90	90	89	90	89
		SVM	72	74	70	70	74
		NN (12)	97	100	95	95	100
	3000–2800 and 1800–900 Combined	J48 Decision Tree	74	81	70	65	84
		RF	87	89	85	85	89
		SVM	56	58	55	55	58
		NN (11)	98	95	100	100	97

Unfavorable region (3000-2800) for generating classification models

Classification models based on neural network (NN) possessed very high accuracy in the range of 90–100% in the 4 region.

In serum:
Best discrimination in serum is in the 1800-900 region by using NN model.

In other region except 3000-2800 region, NN still shows high accuracry 90-100%.

Table 1. Comparison of multiple advanced machine learning algorithms for classification models in serum samples. Abbreviations:Acc—accuracy; Sens—sensitivity; Spec—specificity; PPV—positive predictive value; NPV— negative predictive value; RF—random forest; SVM—support vector machine; NN—neural network. Values in the parentheses after NN indicate the number of hidden layers used in the NN parameter. Values highlighted in grey are the best model in each spectral region.

Result: Classification Model Using Advanced Machine Learning Algorithms

Result: **Exosome**; 70:30 for training and testing

Sample	Region (cm^{-1})	Algorithm	Performance				
			Acc (%)	Sens (%)	Spec (%)	PPV (%)	NPV (%)
Exosome	3000–2800 Lipid	J48 Decision Tree	85	79	93	95	74
		RF	74	75	74	75	74
		SVM	72	71	72	75	68
		NN (14)	77	79	75	75	79
	1800–900 Mixed	J48 Decision Tree	82	81	83	85	79
		RF	90	90	89	90	89
		SVM	74	81	70	65	84
		NN (10)	90	94	86	85	95
	1700–1500 Protein	J48 Decision Tree	67	67	67	70	63
		RF	79	83	76	75	84
		SVM	72	76	68	65	79
		NN (11)	95	95	95	95	95
	1500–900 Fingerprint	J48 Decision Tree	85	94	78	75	95
		RF	87	86	89	90	84
		SVM	72	76	68	65	79
		NN (16)	92	90	94	95	89
	3000–2800 & 1800–900 Combined	J48 Decision Tree	79	83	76	75	84
		RF	90	90	89	90	89
		SVM	82	84	80	80	84
		NN (9)	95	91	100	100	89

Table 2. Comparison of multiple advanced machine learning algorithms for classification models in exosome samples. Abbreviations:Acc—accuracy; Sens—sensitivity; Spec—specificity; PPV—positive predictive value; NPV— negative predictive value; RF—random forest; SVM—support vector machine; NN—neural network. Values in the parentheses after NN indicate the number of hidden layers used in the NN parameter. Values highlighted in grey are the best model in each spectral region.

J48 shows highest accuracy (85%) in the 3000-2800 region

Classification models by the NN algorithm with different hidden layers provide varying accuracy of approximately 90–95%.

RF & SVM algorithm provided the potential for differentiating between 2 groups, with 74–90% and 72–82% respectively.

In the Exosome:
NN shows the best accuracy differentiating between the group in all regions except 3000-2800.

Using lipid region give challenges to differentiate the group but J48 is the best to differentiate.

It is possible to differentiate exosome between 2 groups by using all region

Result: Classification Model Using Advanced Machine Learning Algorithms

Result: **HDL**; 70:30 for training and testing

Sample	Region (cm^{-1})	Algorithm	Performance				
			Acc (%)	Sens (%)	Spec (%)	PPV (%)	NPV (%)
HDL	3000–2800 Lipid	J48 Decision Tree	69	79	64	55	84
		RF	44	45	42	45	42
		SVM	56	56	57	70	42
		NN (8)	72	70	75	80	63
	1800–900 Mixed	J48 Decision Tree	72	74	70	70	74
		RF	85	85	84	85	84
		SVM	74	73	76	80	68
		NN (14)	97	100	95	95	100
	1700–1500 Protein	J48 Decision Tree	79	83	76	75	84
		RF	74	75	74	75	74
		SVM	51	52	50	60	42
		NN (8)	79	77	82	85	74
	1500–900 Fingerprint	J48 Decision Tree	92	95	90	90	95
		RF	90	83	100	100	79
		SVM	77	74	81	85	68
		NN (9)	92	100	86	85	100
	3000–2800 & 1800–900 Combined	J48 Decision Tree	90	94	86	85	95
		RF	82	84	80	80	84
		SVM	69	67	73	80	58
		NN (15)	90	100	83	80	100

Table 3. Comparison of multiple advanced machine learning algorithms for classification models in HDL samples.Abbreviations:Acc—accuracy; Sens—sensitivity; Spec—specificity; PPV—positive predictive value; NPV— negative predictive value; RF—random forest; SVM—support vector machine; NN—neural network. Values in the parentheses after NN indicate the number of hidden layers used in the NN parameter. Values highlighted in grey are the best model in each spectral region.

Various algorithms at lipid region showed unsatisfactory potential for discrimination, with the best accuracy of 72%

NN algorithm was the best algorithm in all regions used. The accuracy performance shown was 72–97%

J48 shows comparable performance to NN in 2 region

In the HDL:
NN algorithm was the best algorithm in all regions used.

Best region of HDL spectra to differentiate between 2 groups is 1800-900.

3000-2800 region one again shows the hardest regions used to differentiate between 2 groups.

Paper 1: Conclusions

- ATR-FTIR combined with advanced machine learning algorithms allows differentiating the elderly with a low percentage (LP) and a high percentage (HP) of pathogenic CD4+ T cells.
- Exosomes are the most likely source of biomarkers (based on PCA and PLS-DA). The use of advanced machine learning algorithms exploring all types of samples (serum, exosomes, and HDL) could be used to classify these two groups.
- The classification models generated by the NN algorithm resulted in the best performance with an accuracy of 100% in serum (1800–900 cm^{-1}), 95% in exosomes (1700–1500 and 3000–2800 and 1800–900 cm^{-1}), and 97% in HDL (1800–900 cm^{-1})

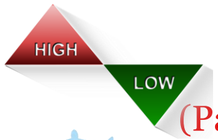

T-Helper Cells:

(Pathogenic CD4+ T-cells)

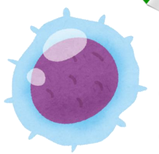

- CD28-
- NKG2D+
- High IL-17 producing cell

Paper 1: Conclusions (cont.)

ATR-FTIR gives advantage

- Ease of handling samples with relatively short measurement duration (only a few minutes)
- Small amount of required sample volume
- Reagent-free approach
- High signal to noise ratio output that facilitates chemometric analysis
- May be suitable for studying multiple biochemical alterations in biological samples where a single FTIR spectrum can provide various biochemical information related to health conditions.

Paper 2: Overview

Nanoscale Horizons

ROYAL SOCIETY OF CHEMISTRY

COMMUNICATION

View Article Online
View Journal | View Issue

Check for updates

Cite this: *Nanoscale Horiz.*, 2022, 7, 1488

Received 3rd May 2022,
Accepted 5th September 2022

DOI: 10.1039/d2nh00220e

rsc.li/nanoscale-horizons

Nanoscale biophysical properties of small extracellular vesicles from senescent cells using atomic force microscopy, surface potential microscopy, and Raman spectroscopy†

Hyo Gyeong Lee,‡[a] Seokbeom Roh,‡[bc] Hyun Jung Kim,[bd] Seokho Kim,[e] Yoochan Hong,*[d] Gyudo Lee*[bc] and Ok Hee Jeon*[a]

What is observed in this study?

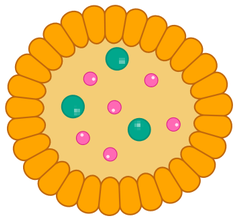

Extracellular Vesicles:

- Microvesicles (lEVs)
- Exosomes (sEVs)
- Carry genetic and molecular information

Objective:

To demonstrate the potential **screening probability** for **differences between sEVs** secreted by ionizing radiation (IR) induced **SnCs and quiescent control cells** (non-SnCs) using atomic force microscopy (AFM), surface potential microscopy, and Raman spectroscopy.

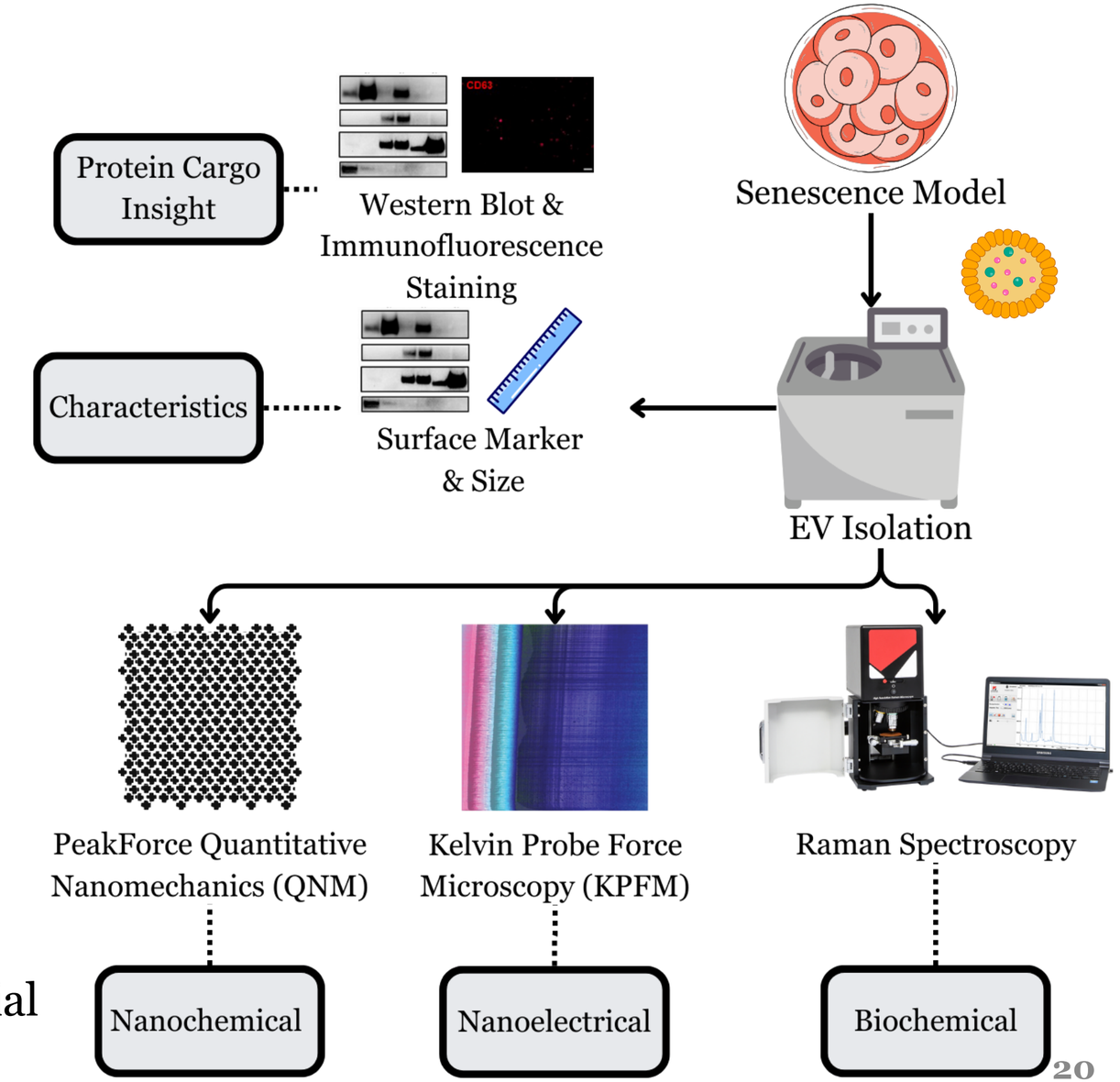

Paper 2: Materials and Methods (Isolation & Confirmation)

EV isolation using differential ultracentrifugation.

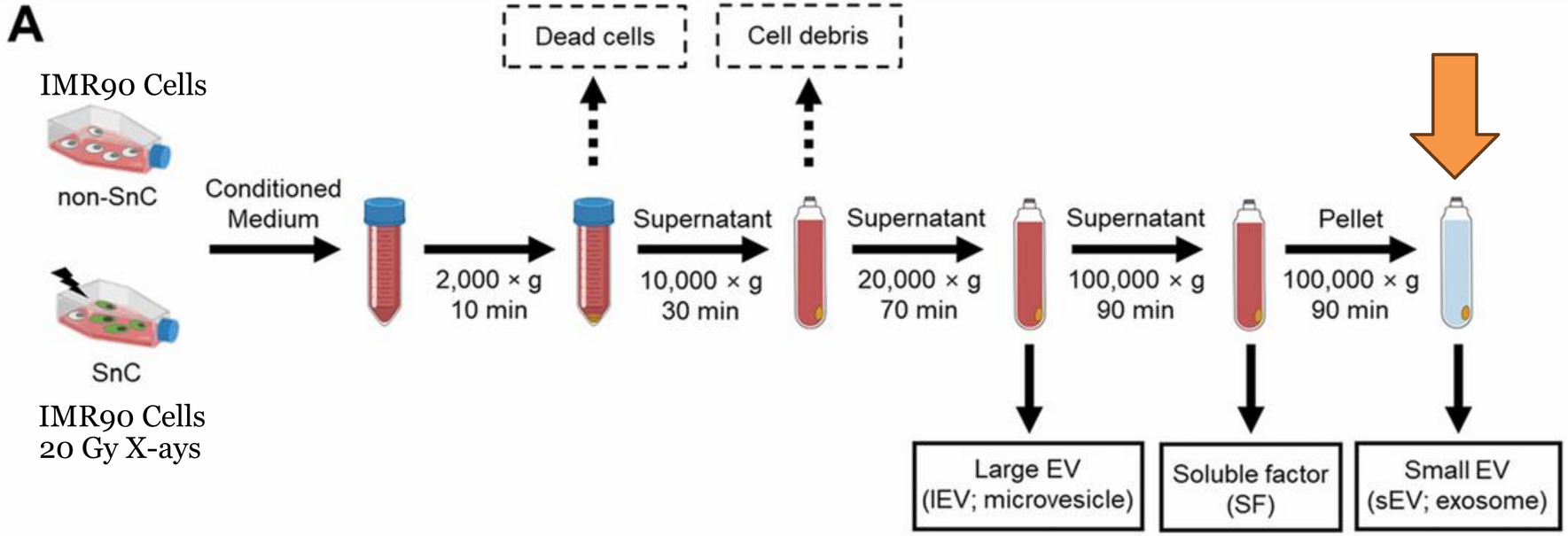

EV analysis: Characteristics, Size, Distribution

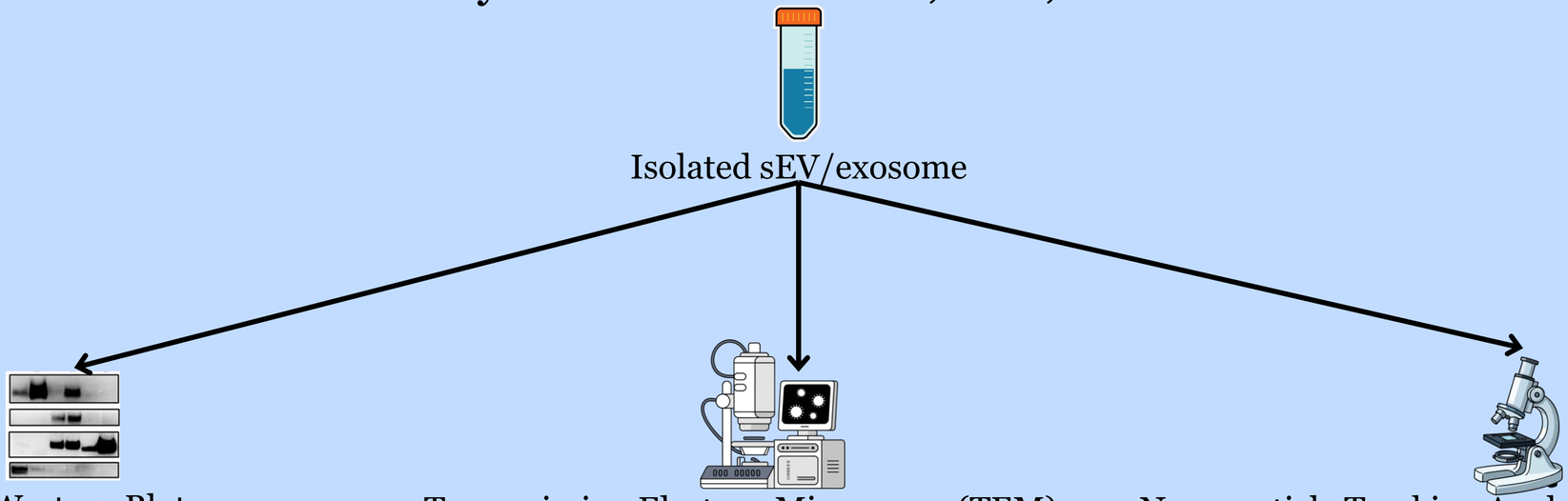

Result: Isolation and analysis of EVs from SnCs

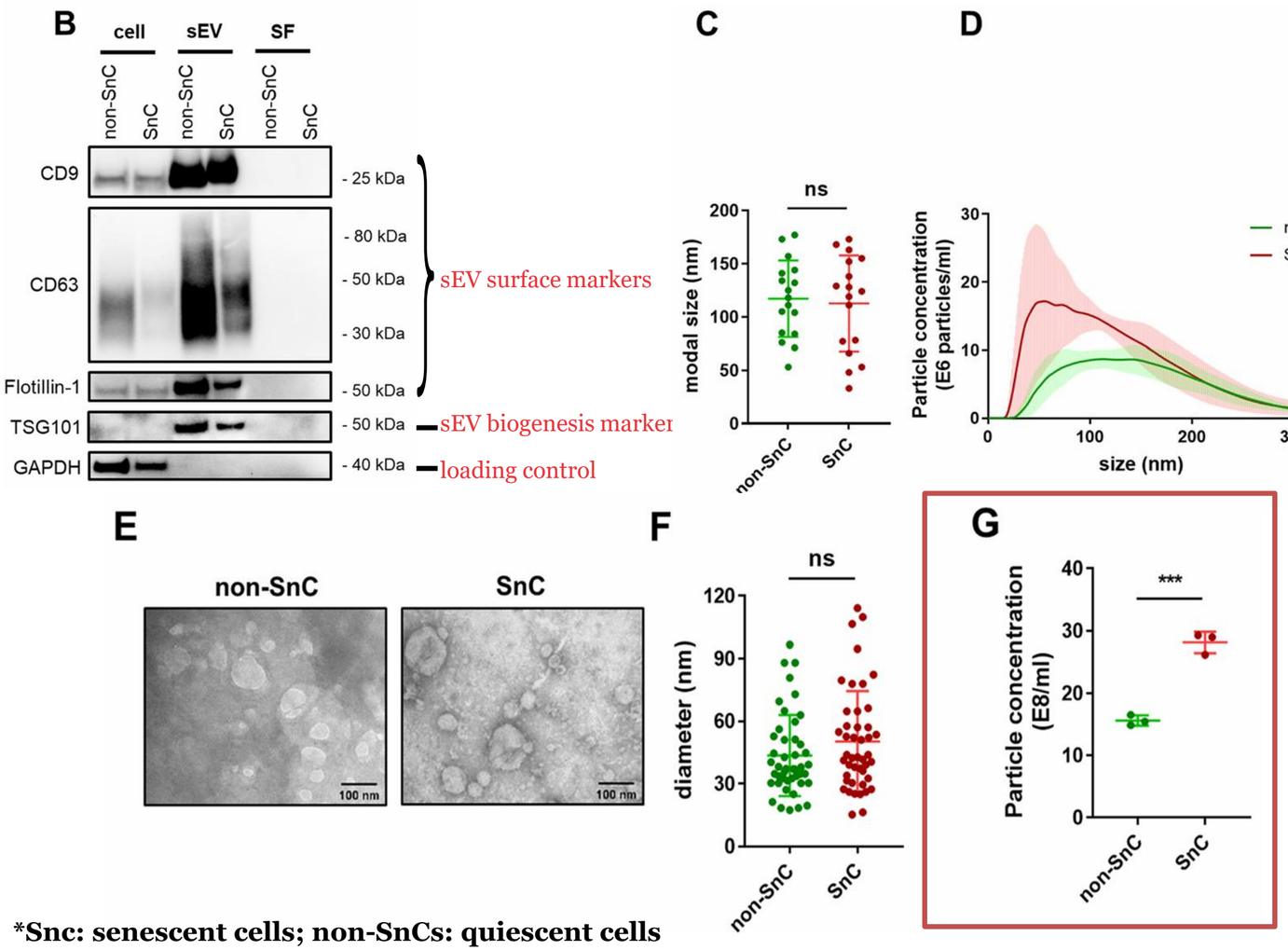

***Snc: senescent cells; non-SnCs: quiescent cells**

***EV: extracellular vesicle; sEV: small extracellular vesicle/exosome; SF: soluble factor**

Fig. 1 Isolation and analysis of sEVs from quiescent (non-SnCs) or senescent cells (SnCs) by differential ultracentrifugation (B) Western blot analysis of cell lysate, sEVs, and soluble factors (SFs) for sEV surface markers CD9, CD63, and flotillin-1 and the sEV biogenesis marker TSG101. GAPDH was used as a loading control. (C) Nanoparticle tracking analysis (NTA) size measurements and (D) size distribution plot of sEVs derived from non-SnC and SnC (n = 17 per group). (E) Representative TEM images of sEVs. Scale bars: 100 nm. (F) Quantification of particle size from TEM images (n = 45 per group). (G) NTA particle concentration measurements of non-SnC and SnC-derived sEVs (n = 3 per group). All values are mean ± S.D. ns: not significant, ***$p < 0.001$. A two-tailed unpaired t-test was used for statistical analysis.

(B). The sEVs derived from the non-SnCs and SnCs expressed:

- Classical sEV surface markers (CD9, CD63, and flotillin-1)
- Bio genesis marker (TSG101)

(C-F).

The sEVs shows **<u>modal sizes</u>** and **<u>size distributions</u>** corresponding to typically **reported sizes** (30–200 nm)

Negligible difference in the diameters of the non-SnC and SnC-derived sEVs (approximately 30–120 nm)

(G).

The secretion of sEVs increased considerably in SnCs

The isolated EV from both senescent and non-senescent cells were confirmed as sEV.

The sEVs was secreted higher in senescent condition

Paper 2: Materials and Methods

Biophysical Properties

Small EV/exosome

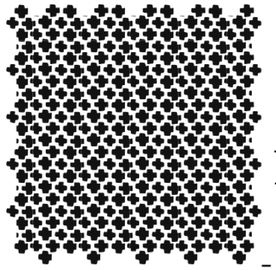

PeakForce Quantitative Nanomechanics (QNM)

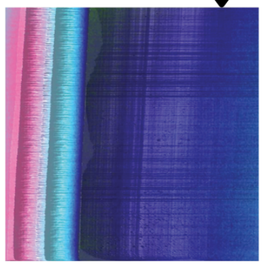

Kelvin Probe Force Microscopy (KPFM)

Raman Spectroscopy

Nanochemical

Nanoelectrical

Biochemical

Result: Mapping of nanomechanical properties of SnC-derived sEVs via PF-QNM

Biophysical properties obtained using PF-QNM

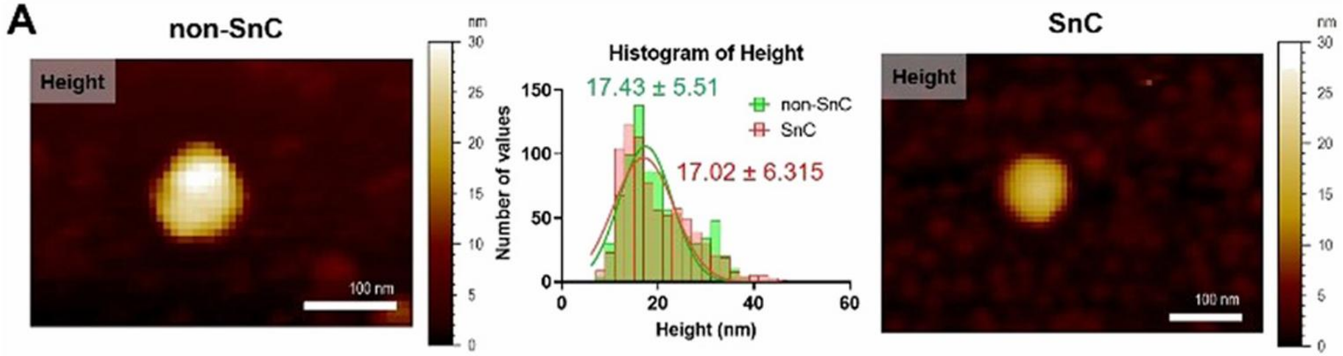

Fig. 2 Biophysical properties obtained using PF-QNM for sEVs from non-SnC (left) and SnC (right). (A) Topographical AFM images

(A).
The height of non-SnC sEV (17.43 nm) (green) and SnC sEV (17.02 nm) (red) was almost similar

Type of sEV	Stiffness (MPa ± S.D.[a])	Deformation (nm ± S.D.)	Adhesion (pN ± S.D.)
Non-SnC	16.10 ± 7.05	1.17 ± 0.49	75.12 ± 21.92
SnC	21.90 ± 9.77	4.10 ± 1.24	170.5 ± 53.98

Table 1 Nanomechanical properties of non-SnC- and SnC-derived sEVs, obtained from histograms by fitting a Gaussian function

(Table 1).
SnC-derived sEVs increased in stiffness, had larger deformation, and higher adhesion value (significant).

sEV from different source had similar size, however they have different biophysical properties.

This may suggest a changes in the biomolecular content (cargo) of the sEV derived from senescent cells

Result: Mapping of the nanoelectrical properties of SnC-derived sEVs by KPFM

Nanophysical properties obtained using KPFM

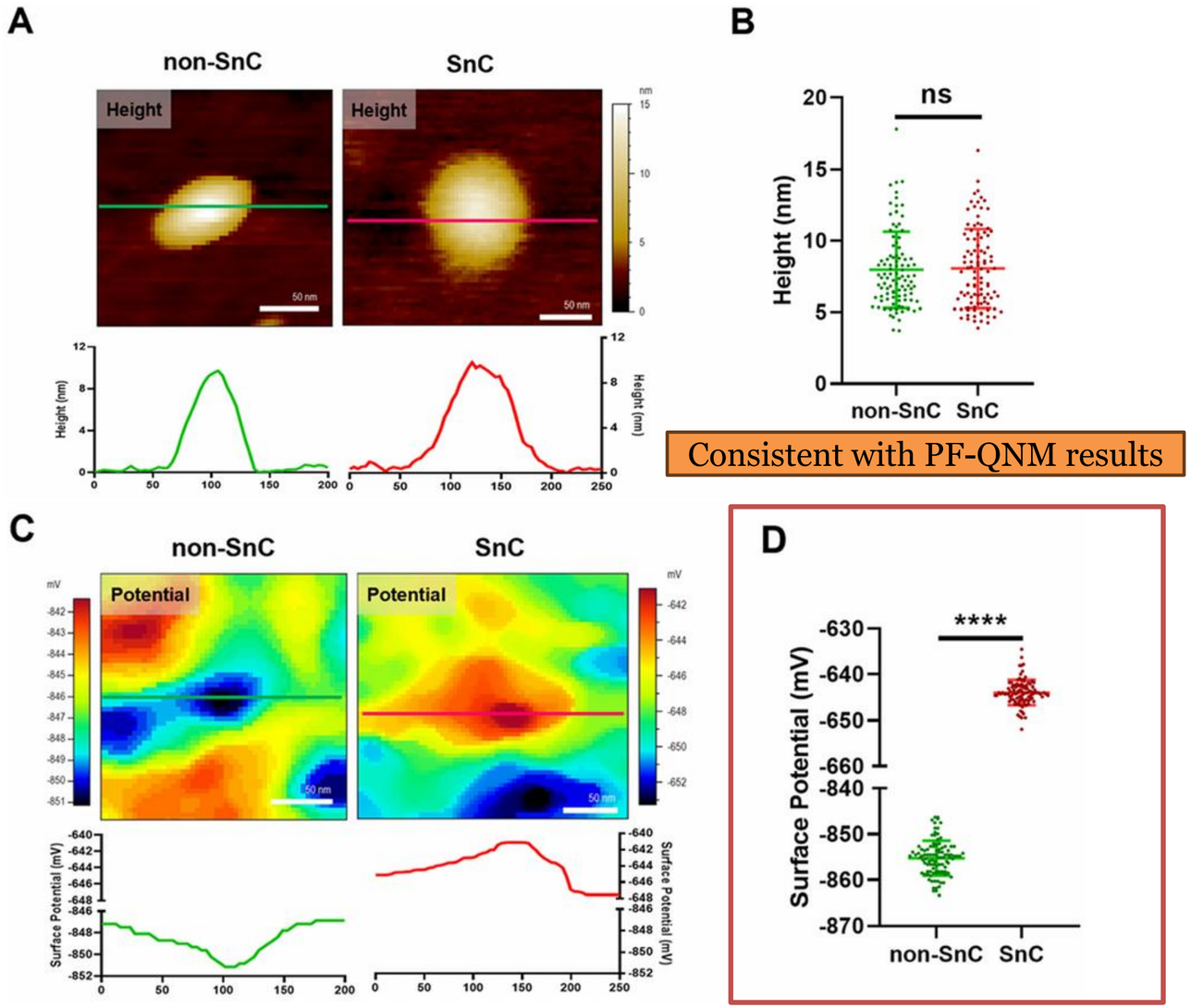

Consistent with PF-QNM results

(A)&(B)
There was no significant difference in the sizes of sEVs obtained through KPFM between non-SnC-derived sEVs (8.0 ± 2.7 nm) and SnC-derived sEVs (8.1 ± 2.8 nm). Consistent with that of the PF-QNM results

(C)&(D)
A significant difference in the surface potential was observed by KPFM between non-SnC-derived sEVs (−855.2 ± 3.8 mV) and SnC-derived sEVs (−643.9 ± 2.7 mV)

These results suggest that cellular senescence altered the membrane composition of sEVs secreted by cells.

Surface potential of sEVs is associated to changes in their composition of the sEV membrane

Fig. 3 Analysis of KPFM for physical and electrical properties of sEVs isolated from non-SnCs and SnCs. (A) Topographical AFM images of a single non-SnC-derived sEVs and SnC-derived sEVs. Line profiles of each image are depicted below. (B) Quantification of the height of sEVs derived from non-SnCs and SnCs (n = 100 per group). (C) Electrical property mapping of a single non-SnC-derived sEV and SnC-derived sEVs. Line profiles of each image are shown below. (D) Quantification of the surface potential of sEVs from non-SnCs and SnCs (n = 100 per group). ns: not significant, ****$p < 0.0001$. A two-tailed unpaired t-test was used for statistical analysis.

Result: Biochemical features of SnC-derived sEVs using Raman spectroscopy

Biochemical by Raman spectroscopy (100 spectra each)

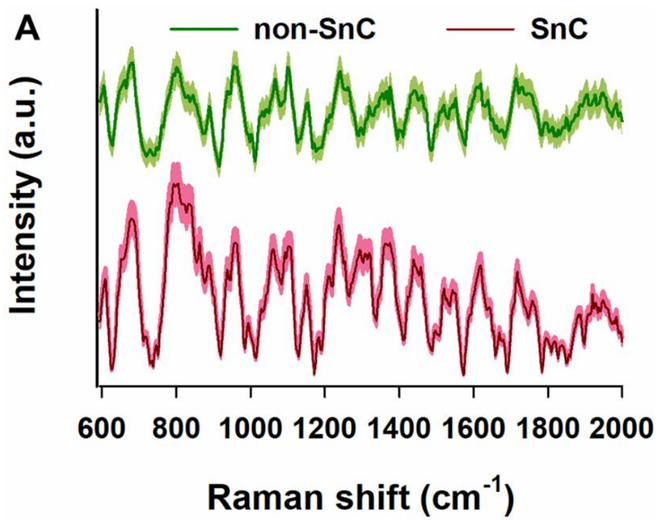

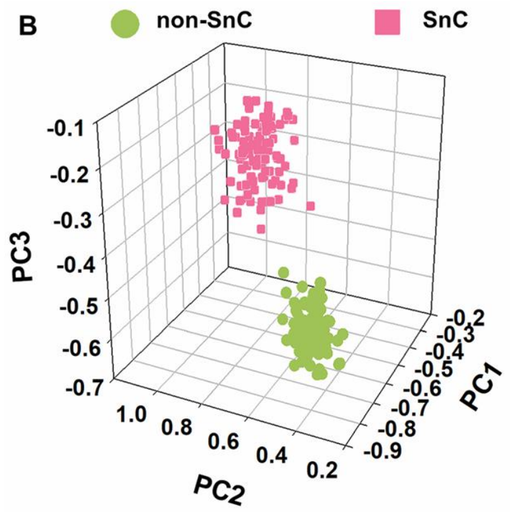

(A). Striking variability of raman spectra from the non-SnC and SnC-derived sEVs.

(B). There was a difference in PC3 between non-SnC- and SnC-derived sEVs

(C). sEVs secreted from SnCs had more summation of (+) charged amino acids compared to those secreted from non-SnCs

(D). The ratio (+ to -) was higher for the sEVs secreted from SnCs than for the sEVs secreted from non-SnCs

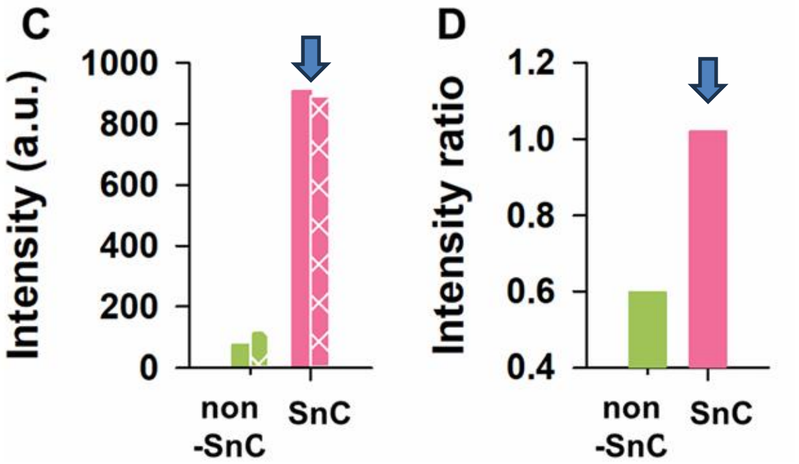

- **Distinct biochemical profile** of the sEVs secreted by non-SnCs and SnCs
- **Possible to differentiate** the sEV from both group by PCA analysis
- Many **positively charged** substances were distributed **on the surfaces** of the **SnC-derived sEVs**, consistent with the AFM results

***non-pattern: positive (+) charge; pattern: negative (-) charge**

Fig. 4 Analysis of SnC-derived sEVs using Raman spectroscopy. (A) Raman spectra (solid lines) and ±5% standard deviation (shaded area) of sEVs from non-SnC and SnC. (B) A plot of 3D-PCA scores with the first, second, and third principal components (PCs) for individual Raman spectra. (C) Raman intensities of characteristic peaks for (+) and (−) charged amino acids. Non-patterned and patterned bar plots represent the summation of the Raman intensities at characteristic peaks of (+) and (−) charged amino acids, respectively. (D) Raman intensity ratios of (+) and (−) charged amino acids, using each value of summation of Raman intensities at the characteristic peaks for (+) and (−) charged amino acids.

Paper 2: Materials and Methods

Cargo Proteins Identities: Target Selection

Published proteomic sEV data
(irradiated senescent fibroblasts)

- pI value
- Charge at pH 7.4
- Fold Change

IGFBP7
Gremlin-1
Annexin II

- senescence growth arrest,
- senescence-related proinflammation
- key exosomal SASPs (aging & related inflammatory diseases)

Cargo Proteins Identities: Target Selection

Small EV/ exosome

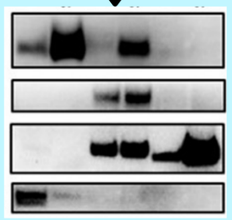

Western Blot

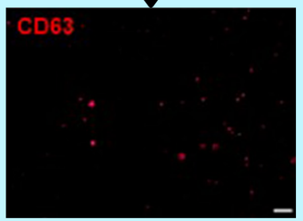

Immunofluorescence Staining

Bulk Analyses

Single Analysis

Result: Analysis of a select group of positively charged SASP proteins in SnC-derived sEVs

Result: Analysis of a selected proteins enriched in SnC-derived sEV (WB)

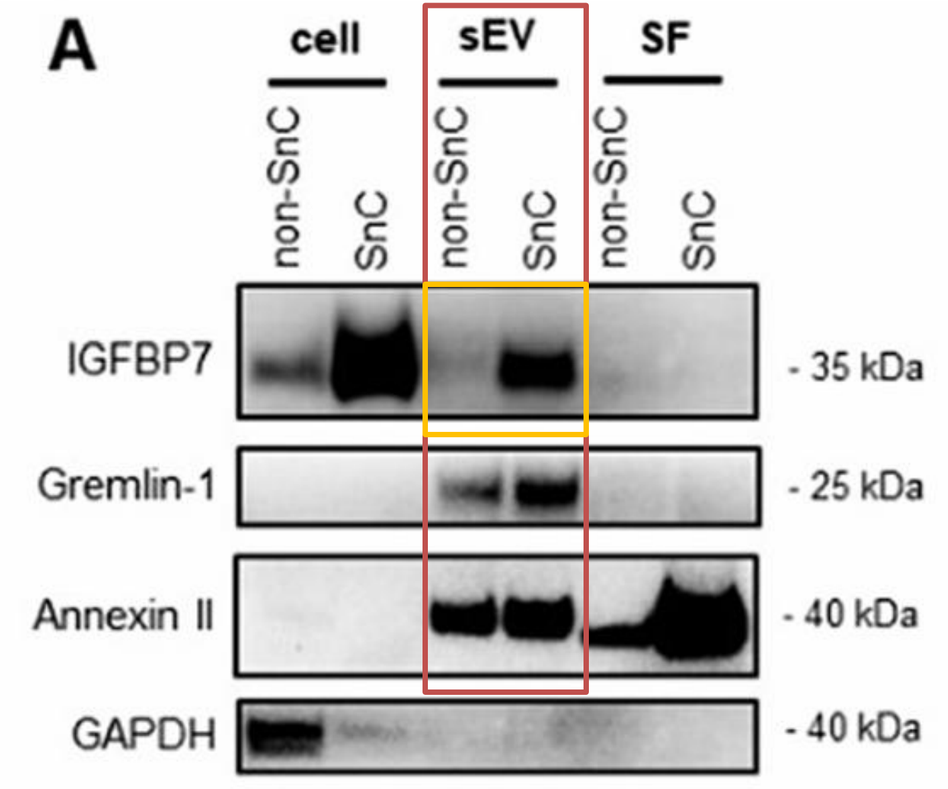

Fig. 5 Analysis of a select group of positively charged proteins enriched in SnC-derived sEV. (A) Western blot analysis of cell lysate, sEV, and SFs for IGFBP7, gremlin-1, and annexin II. GAPDH was used as a loading control.

*sEV: small extracellular vesicle/exosome; SF: soluble factor

(A). Levels of IGFBP7, gremlin-1, and annexin II increased markedly in SnC-derived sEVs

<u>Inconclusive</u>

All or only some SnC-derived sEV subsets carried IGFBP7, gremlin-1, and annexin II

Senescent cause changes (increase) in the protein content of sEV

Result: Analysis of a select group of positively charged SASP proteins in SnC-derived sEVs (cont.)

Result: Analysis of a selected proteins enriched in SnC-derived sEV (IF)

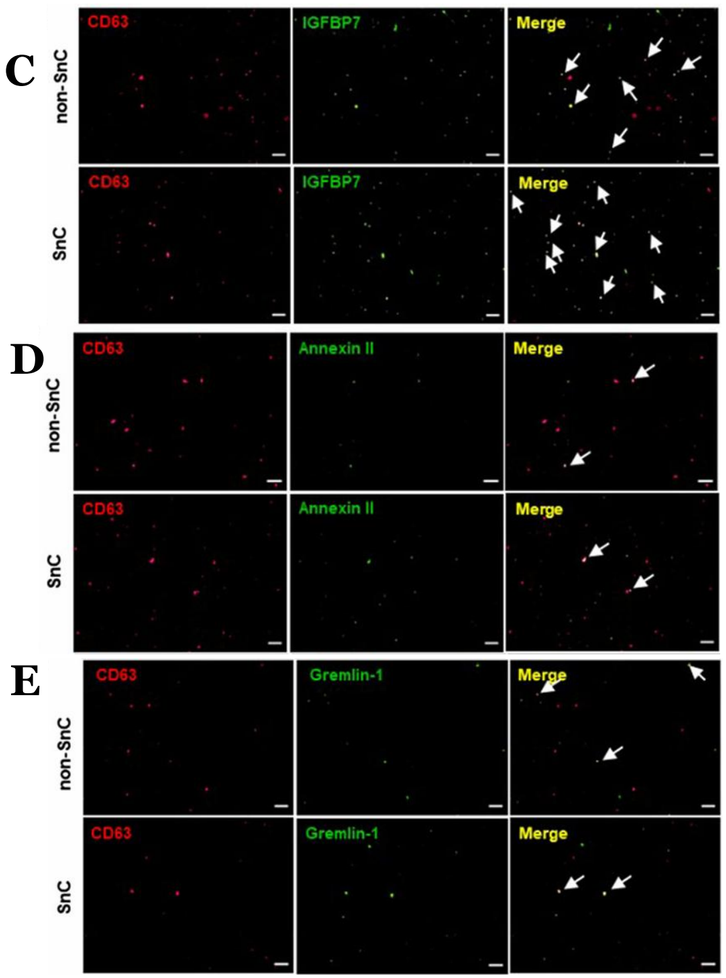

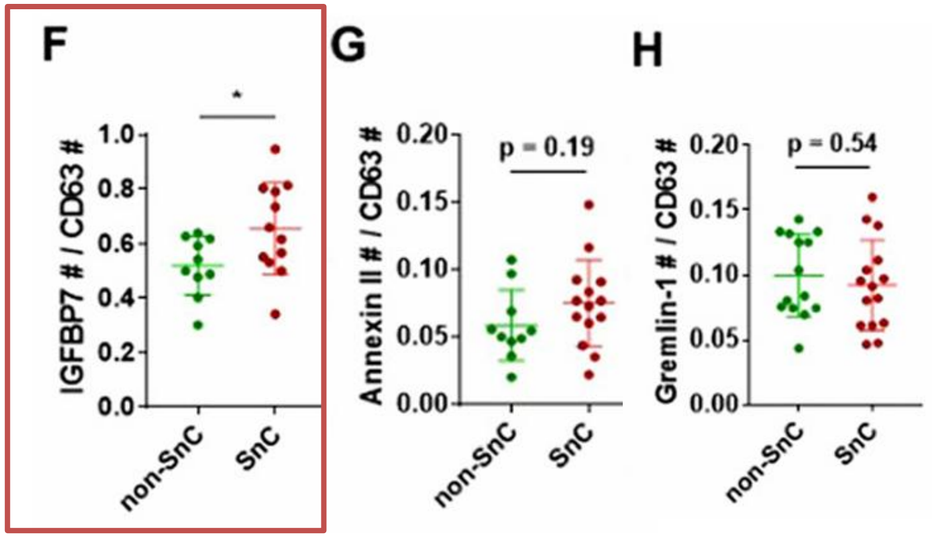

Markers:

- CD63 (red, sEV marker)
- (**C**) IGFBP7 (green, cargo protein of sEV)
- (**D**) annexin II (green, cargo protein of sEV)
- (**E**) gremlin-1 (green, cargo protein of sEV)

(C-H)
Total number of IGFBP7- and annexin II-carrying CD63+ vesicles tended to increase, but the difference was not significant in gremlin-1-carrying CD63+ vesicles

Three positively charged proteins—may be factors contributing to their distinct biophysical and biochemical characteristics at the nanoscale.

Fig. 5 (cont.) (C) IGFBP7 (green, cargo protein of sEV), (D) annexin II (green, cargo protein of sEV) or (E) gremlin-1 (green, cargo protein of sEV) shown separately or as a merged image. In the merged image, arrows indicate double-positive sEVs. Scale bar: 10 μm. (F)–(H) Quantification of co-stained CD63-positive (n > 10 images per group) and cargo protein-positive sEV (n > 10 images per group). All values are mean ± S.D. ns: not significant, *p < 0.05. A two-tailed unpaired t-test was used for statistical analysis.

Paper 2: Conclusion

- Three combined techniques (QNM, KPFM, Raman spectroscopy) can be used for the high-resolution and multi-parameter characterization of SnC-derived sEVs. Furthermore, these 3 method can be used to investigate the biophysical features of SnC-derived sEVs, without specific biomarkers.
- The biophysical properties of sEVs can be a hallmark of cellular senescence and can be applied to develop noninvasive, safe, and sensitive analytical methods to scrutinize SnC-derived sEVs in cell culture, as well as in clinical samples such as plasma from patients with age-related diseases.

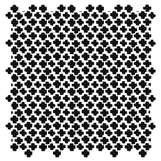

PeakForce Quantitative Nanomechanics (QNM)

Kelvin Probe Force Microscopy (KPFM)

Raman Spectroscopy

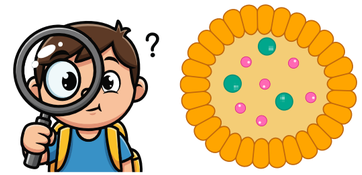

SnC-derived sEVs

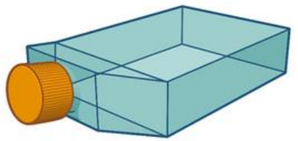

Noninvasive

Safe

Sensitive

Criticism

	Strengths	Weaknesses
Paper 1	• The study demonstrates the potential use of ATR-FTIR to discriminate samples with high and low percentage of immunosenescent cells	• Number of spectra used only 129, where ideally is 1,000 samples for SVM and NN algorithm.
Paper 2	• The study demonstrate the potential use of Raman Spectroscopy, KPFM, ATM to measure senescent condition in the sample… additionally give marker of senescence	• The study was conducted using *In vitro* samples • No further confirmation of protein content in the other sEVs subsets

References

Introduction:

Bai, A., Moss, A., Rothweiler, S., Serena Longhi, M., Wu, Y., Junger, W. G., & Robson, S. C. (2015). NADH oxidase-dependent CD39 expression by CD8+ T cells modulates interferon gamma responses via generation of adenosine. Nature communications, 6(1), 8819.

Canale, F. P., Ramello, M. C., & Montes, C. L. (2018). CD39 as a marker of pathogenic CD8+ T cells in cancer and other chronic inflammatory diseases. Oncoscience, 5(3-4), 65.

Gupta, P. K., Godec, J., Wolski, D., Adland, E., Yates, K., Pauken, K. E., ... & Haining, W. N. (2015). CD39 expression identifies terminally exhausted CD8+ T cells. PLoS pathogens, 11(10), e1005177.

Putri, P. H. L., Alamudi, S. H., Dong, X., & Fu, Y. (2025). Extracellular vesicles in age-related diseases: disease pathogenesis, intervention, and biomarker. *Stem Cell Research & Therapy*, *16*(1), 263.

Shaw, A. C., Joshi, S., Greenwood, H., Panda, A., & Lord, J. M. (2010). Aging of the innate immune system. Current opinion in immunology, 22(4), 507-513.

Sornkayasit, K., Jumnainsong, A., Phoksawat, W., Eungpinichpong, W., & Leelayuwat, C. (2021). Traditional Thai massage promoted immunity in the elderly via attenuation of senescent CD4+ T cell subsets: a randomized crossover study. *International Journal of Environmental Research and Public Health*, *18*(6), 3210.

Phoksawat, W., Jumnainsong, A., Sornkayasit, K., Srisak, K., Komanasin, N., & Leelayuwat, C. (2020). IL-17 and IFN-γ productions by CD4+ T cells and T cell subsets expressing NKG2D associated with the number of risk factors for cardiovascular diseases. *Molecular Immunology*, *122*, 193-199.

Phoksawat, W., Jumnainsong, A., Leelayuwat, N., & Leelayuwat, C. (2017). Aberrant NKG2D expression with IL-17 production of CD4+ T subsets in patients with type 2 diabetes. *Immunobiology*, *222*(10), 944-951.

Sornkayasit, K., Leelayuwat, C., Jumnainsong, A., Tippayawat, P., Wongfieng, W., Praja, R. K., ... & Phoksawat, W. (2025). Predominant expression of the immunosenescent biomarker CD57 on CD4+ T cells and their subsets in the older people associating with the cardiovascular disease risk factors. *Journal of Leukocyte Biology*, *117*(9), qiaf124.

Weksler, M. E. (2000). Changes in the B-cell repertoire with age. Vaccine, 18(16), 1624-1628.

Zhang, J., He, T., Xue, L., & Guo, H. (2021). Senescent T cells: a potential biomarker and target for cancer therapy. *EBioMedicine*, *68*.

Seminar Paper:

Praja, R. K., Wongwattanakul, M., Tippayawat, P., Phoksawat, W., Jumnainsong, A., Sornkayasit, K., & Leelayuwat, C. (2022). Attenuated Total Reflectance-Fourier Transform Infrared (ATR-FTIR) Spectroscopy Discriminates the Elderly with a Low and High Percentage of Pathogenic CD4+ T Cells. Cells, 11(3), 458.

Lee, H. G., Roh, S., Kim, H. J., Kim, S., Hong, Y., Lee, G., & Jeon, O. H. (2022). Nanoscale biophysical properties of small extracellular vesicles from senescent cells using atomic force microscopy, surface potential microscopy, and Raman spectroscopy. Nanoscale horizons, 7(12), 1488-1500.

Acknowledgement

Advisor

Asst. Prof. Wisitsak Phoksawat

1st Year Master Student